Structural and optical behavior of SnS$_2$/NiFe$_2$O$_4$ NCs prepared via novel two-step synthesis approach for MB and RhB dye degradation under sun light irradiation

K. S. Ashraff Ali^1 · V. Mohanavel^2 · C. Gnanavel^3 · V. Vijayan^4 · N. Senthilkumar^5

Abstract

The present investigation focuses on facile two-step synthesis approach fabrication of tin sulfide (SnS$_2$)/ nickel ferrite (NiFe$_2$O$_4$) nanocomposites (NCs) for the first time. The crystallinity and phase purity of the prepared material was investigated in powder X-ray diffraction (PXRD) studies. The presence of functional groups (stretching and bending vibration) was primarily determined by the Fourier Transform Infrared Spectroscopy (FT-IR) analysis. As well as, optical behavior of the synthesized samples was determined in UV–Vis absorption spectroscopic studies, and the presence of surface defects was established by PL spectroscopic studies. From the FESEM analysis, sponge-like structure was attained and Ni, Fe, Sn, S and O elemental component was determined by the EDAX spectrum analysis. The as-prepared SnS$_2$/NiFe$_2$O$_4$ NCs exhibit superior photocatalytic performance and high stability toward the reduction of methylene blue (MB) and rhodamine B (RhB) dyes under irradiation of direct sunlight. The synthesized nanocomposites showed an efficient photocatalytic activity with a high reaction kinetic rate.

Keywords SnS$_2$/NiFe$_2$O$_4$ NCs · Two-step synthesis approach · Structural · Optical · Photocatalytic activity

✉ K. S. Ashraff Ali
  ashraffali1986@gmail.com

1 Department of Mechanical Engineering, C. Abdul Hakeem College of Engineering & Technology, Melvishram, Vellore 632509, Tamil Nadu, India

2 Department of Mechanical Engineering, Bharath Institute of Higher Education and Research, Chennai 600073, Tamil Nadu, India

3 Department of Mechanical Engineering, Vels Institute of Science, Technology and Advanced Studies, Chennai 600117, Tamil Nadu, India

4 Department of Mechanical Engineering, K.Ramakrishnan College of Technology, Samayapuram, Trichy 621112, Tamil Nadu, India

5 Department of Electronics and Communication Engineering, M.Kumarasamy College of Engineering, Karur 639113, Tamil Nadu, India

Introduction

In recent decade, various developments in industries have created major environmental problems due to contamination of water by organic or synthetic pollutants [1, 2]. Predominantly, leather, textile, chemical, paper, pharmaceutical and cosmetic industries are releasing waste dye waters that demonstrate extreme coloration in the water ecosystem [1]. Therefore, removal of inorganic and organic dyes from the effluents is a challenge posed to everyone currently [3]. Hence, numerous researchers have endeavored some remedial methods, such as chemical, physical, biological, UV and visible light-based treatment methods to eradicate the water pollution and sustain the available water sources for future generation [4–10]. Thus, the photocatalysis process is one of the most important techniques for purification of waste dye water due to its low maintenance cost, posttreatment management of by products and high energy consumption, compromising of limitation in complete decontamination [1].

In current era, nanosized metal oxide semiconductors TiO_2, ZnO, CdO, WO_3, Fe_2O_3, Bi_2O_3 CdS, ZnS and SnS_2, etc. are extensively investigate photocatalytic activity owing to their chemical stability, band gap, nontoxicity and inertness [11, 12]. Among them, tin disulfide (SnS_2) is an important CdI_2-type IV–VI group layered n-type semiconductor with a narrow band gap of about 2.18–2.44 eV [12]. Due to its noticeable high theoretical capacity, optical absorption coefficient and charge mobility have probable capability in anode for lithium-ion batteries, solar cells, optoelectronic devices, field-effect transistors, gas sensors, etc. [13, 14]. The SnS_2 exhibits oxidation resistance in the photocatalytic reactions owing to its inexpensive, good acidic thermal stability and oxidative nature [15]. Thus, it acts as a promising visible light-sensitive photocatalyst.

In recent days, NiFe oxide-based semiconductor photocatalysts have paid much attention in the field of heterogeneous photocatalysis [16]. Because, nanocatalysts are easily recover after the photocatalytic reaction by applied external magnetic field [16]. Among that, inverse spinel nickel ferrite ($NiFe_2O_4$) attracts the researchers owing to their outstanding ferromagnetic property, low cost, narrow direct band gap (2.19 eV) as well as good chemical and thermal stability [16]. However, $NiFe_2O_4$ exhibit week photocatalytic activity due to their fast recombination of photo-generated electron–hole pair under visible light irradiation. Hence, considering their individual characteristics of the semiconductor (SnS_2), the coupling between two different semiconductors (SnS_2 and $NiFe_2O_4$) were give rise to enhancement in the photocatalytic efficiency due to its photoinduced electrons and holes are separated effectively via interfacial charge transfer [17]. In the aspect, Guo et al. has developed p-Ag_2O/n-$ZnFe_2O_4$ heterostructure for better performance toward the degradation of BPA under visible light illumination due to their quick separation of photogenerated charge carrier [18].

Therefore, the photocatalytic activity has been investigated from the developed $SnS_2/NiFe_2O_4$ nanocomposites (NCs) for degradation of methylene blue (MB) and rhodamine B (RhB) organic dyes under simulated sunlight irradiation. To the

best of our knowledge, the existing reports have not been studied so far in the formation of such nanocomposites.

Experimental procedure

Materials for synthesizing of SnS$_2$/NiFe$_2$O$_4$ NCs

The Nickel (II) nitrate hexahydrate (Ni(NO$_3$)$_2$·6H$_2$O), ferric (III) nitrate nonahydrate (Fe(NO$_3$)$_3$·9H$_2$O) and stannic chloride pentahydrate (SnCl$_4$·5H$_2$O) were used as the precursor material for develop the SnS$_2$/NiFe$_2$O$_4$ NCs. The ammonia solution (NH$_4$OH) and thioacetamide (C$_2$H$_5$NS) performs as a reducing agent. The Cetyl trimethyl ammonium bromide (CTAB) (C$_{19}$H$_{42}$BrN) acts as the capping agent. Double distilled (DD) water was used as a solvent in overall experimental studies. The utilized organic dyes (methylene blue and rhodamine B) and chemicals were received from Merk.

Synthesis procedure for NiFe$_2$O$_4$ nanoparticles

The preparation of NiFe$_2$O$_4$ (Nickel ferrite) NP was carried out by a simple chemical co-precipitation technique, and the synthesis procedure is narrated in the following sections. Initially, 0.2 M (12.1 gm) of Fe (NO$_3$)$_3$·9H$_2$O and 0.1 M (4.3 gm) of Ni (NO$_3$)$_2$·6H$_2$O was taken and dissolved in 150 ml of DD water. The reaction solution present in the beaker was vigorously stirred for 30 min to achieve a homogenous mixture. A 50 ml of 25% (NH$_4$OH) aqueous ammonia solution was added slowly into the above mixture. The addition of ammonia solution is completed, and the reaction mixture has been stirred continuously for 7 h. The stirrer is stopped, and then the beaker containing the reaction mixture is kept separately without any disturbances for 12 h. Now, the precipitate was slowly and completely been settled at the bottom of the beaker. The wet precipitate is collected and washed with ethanol using filter paper. Then, the precipitate is collected in a petri dish. The petri dish is kept in a hot air oven for 12 h at 80 °C for the purpose of drying. The obtained material is powdered and kept in a muffle furnace for 3 h at 700 °C for calcination.

Synthesis technique for SnS$_2$/NiFe$_2$O$_4$ NCs:

For the fabrication of SnS$_2$/NiFe$_2$O$_4$ NCs, 1 g of already prepared NiFe$_2$O$_4$ NPs was poured in 100 ml of DD water and ultrasonicate for 45 min in order to attain a complete dispersion of NPs in the water. About 2 g of SnCl$_4$·5H$_2$O and 0.05 M of C$_{19}$H$_{42}$BrN was well-dissolved in 50 ml of DD water to make aqueous homogenous solution and added slowly in to the beaker containing NiFe$_2$O$_4$ mixture. After this addition, the entire solution is thoroughly mixed by vigorous stirring for 45 min. A 50 ml of 0.1 M of C$_2$H$_5$NS aqueous solution was added slowly into the reaction mixture. The process was completed, and the whole mixture is vigorously stirred for 7 h. The stirrer is stopped, and then the beaker containing the reaction mixture is kept

separately without any disturbances for 12 h. Now, the precipitate was slowly and completely been settled at the end of the beaker. The wet precipitate is collected and washed with ethanol using filter paper, and then the precipitate is collected in a petri dish. The petri dish is kept in a hot air oven at 100 $^\circ$C for 12 h.

Analytical techniques

The presence of composition, crystallinity and crystalline phases were investigated in PXRD measurement from the instrument model of Pro Penalty CAL (Cu-Kα radiation (1.5406 Å)). The observed various functional groups in the prepared samples were examined in KBr pellet technique by FT-IR (TENSOR 27) Spectrometer (Bruker). The optical performance of SnS_2/$NiFe_2O_4$ NCs was explored by UV–Visible (JASCO V-670) spectrometer. To evaluate the surface morphology and distribution of elemental component in the surface of the prepared SnS_2/$NiFe_2O_4$ NCs was analyzed by FESEM and EDAX color mapping which was carried out by the instrument of Zeiss Gemini Ultra-55 instrument model.

Experimental procedure for Photocatalytic test

The photocatalytic ability of the prepared samples was studied experimentally using MB and RhB dyes as an organic pollutant. About 20 mg/l concentration and 100 ml of each dye solution were taken separately as initial concentration, and then 5 mg of prepared samples were taken as nano photocatalyst. The sunlight is utilized as the photo source for the degradation of dye molecules. The aliquots of each dye were taken at regular intervals and subjected to UV–Visible spectroscopy for analyzing the percentage of degradation and rate constant for the degradation of dye molecules by the prepared photocatalyst. The experiment was carried out on a perfect sunny day at noontime, that is, between 12.00 and 2.00 pm for the purpose of maximum utilization of sunlight and the intensity was ~975 W m^{-2}. The degradation efficiency of the prepared samples was estimated by the given traditional formula,

$$R = \left[(C_0 - C_t)/C_0 \right] \times 100\%,$$

 where C_0 is the opening concentrations of MB &RhB and C_t is the concentration of the dyes with respect to time, respectively.

Results and discussion

Structural analysis

Figure 1 reveals the typical PXRD pattern for as-synthesized $NiFe_2O_4$ and SnS_2/$NiFe_2O_4$ NCs. The sharp and narrow diffraction peak positions are located at 2θ values 18.53°, 30.64°, 36.14°, 37.72, 43.67°, 54.18°, 57.73° and 63.33° which are individually indexed with the (111), (220), (311), (222), (400), (422), (511) and (440) hkl planes, which can be consistent with the cubic spinel phase and space group
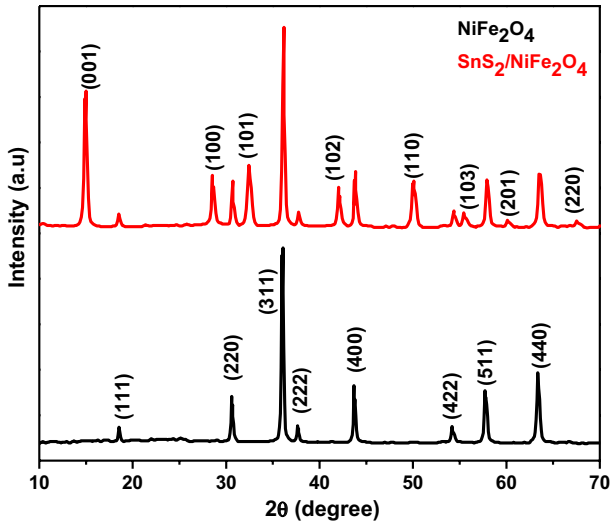
Fig. 1 Powder X-ray diffraction pattern of NiFe$_2$O$_4$ and SnS$_2$/NiFe$_2$O$_4$ NCs

Fd-3 m of NiFe$_2$O$_4$, respectively JCPDS no: 54–0964 [17]. The secondary phase of hexagonal structured diffraction peaks was noticed for pure SnS$_2$ (JCPDS Card No. 23–0677) [12]. The average crystallite size of the NiFe$_2$O$_4$ and SnS$_2$/NiFe$_2$O$_4$ NCs was determined from the most intense reflection using Debye–Scherrer's formula ($D_c = K\lambda/\beta \cos\theta$) [19, 20]. The average grain size of the prepared NiFe$_2$O$_4$ and SnS$_2$/NiFe$_2$O$_4$ NCs was estimated as to be 36 nm and 42 nm, respectively. As well as, no obvious peaks of impurities, such as iron, tin and nickel oxides, were exist from the PXRD pattern, which primarily demonstrates that the impurity free SnS$_2$/NiFe$_2$O$_4$ NCs was formed. In dislocation density (δ), crystallographic defects that strongly induced from the developed materials which were evaluated by specified relation

$$\delta = \frac{1}{D^2},$$

where D denotes the crystallite size. The dislocation density (δ) of the NiFe$_2$O$_4$ and SnS$_2$/NiFe$_2$O$_4$ NCs were attained to be 7.71 10^{-4}(nm)$^{-2}$ and 5.66 10^{-4}(nm)$^{-2}$ [21–24].

Fourier Transform Infrared Spectroscopy (FT-IR) Analysis

Figure 2 reveals the FT-IR spectrum of prepared NiFe$_2$O$_4$ and SnS$_2$/NiFe$_2$O$_4$ NCs. A peak arising at 3557 cm^{-1} is attributed due to O–H stretching mode which clearly demonstrates that the existence of water molecules absorbed on the surface of synthesized nanomaterials [11]. The peak appeared at 662 cm^{-1} is originating by the formation of Sn-S bond [15]. The two peaks appearing at 538 and 415 cm^{-1} are ascribed to the stretching vibration bonds between nickel
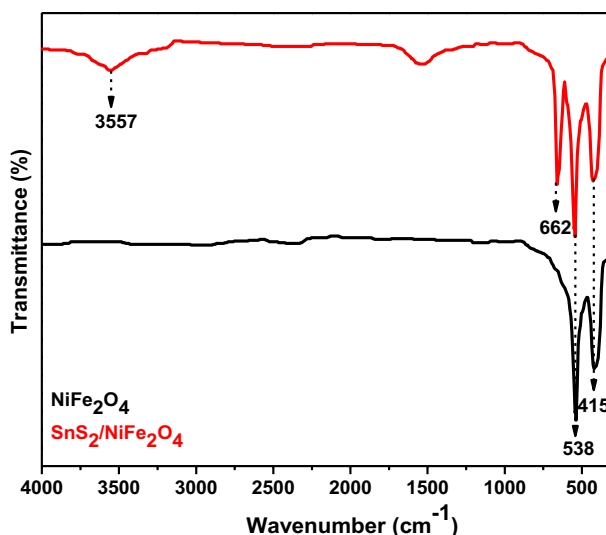
Fig. 2 FT-IR spectrum of $NiFe_2O_4$ and $SnS_2/NiFe_2O_4$ NCs

and oxygen ions (Ni–O) of tetrahedral sites in association with the stretching vibration bonds between iron and oxygen ions (Fe–O) of octahedral complexes, respectively. These are indication of the formation of spinel ferrite structure [25, 26].

Optical study

Optical absorption studies

Figure 3a revealed the optical absorbance spectra of $NiFe_2O_4$ and $SnS_2/NiFe_2O_4$ NCs. The optical band gap energy (Eg) was primarily investigated via developed $NiFe_2O_4$ and $SnS_2/NiFe_2O_4$ NCs material from Tauc's relation:

$$(\alpha h\upsilon)^2 = A\left(h\upsilon - E_g\right),$$

where 'A' signifies as absorption constant with respect to transition probability, 'hυ' and 'α' represents as incident photon energy and absorption coefficient [19–21]. From the Tauc's plot, Eg values of the samples were determined from a deviation of plot $(\alpha h\upsilon)^2$ versus photon energy (hυ) as presented in Fig. 3b. The band gap was achieved to be 1.51 eV and 1.74 eV, respectively, for $NiFe_2O_4$ and $SnS_2/NiFe_2O_4$ NCs. Compared to the $NiFe_2O_4$, the absorption spectra of hybrid combination have higher band gap due to their effective charge exchange from the $NiFe_2O_4$ to the SnS_2, and it suppresses recombination of electron–hole pairs in the composite [17]. Thus, significant enhancement was observed from the results of $SnS_2/NiFe_2O_4$ NCs in the photocatalytic processes under illumination of sun's radiation.

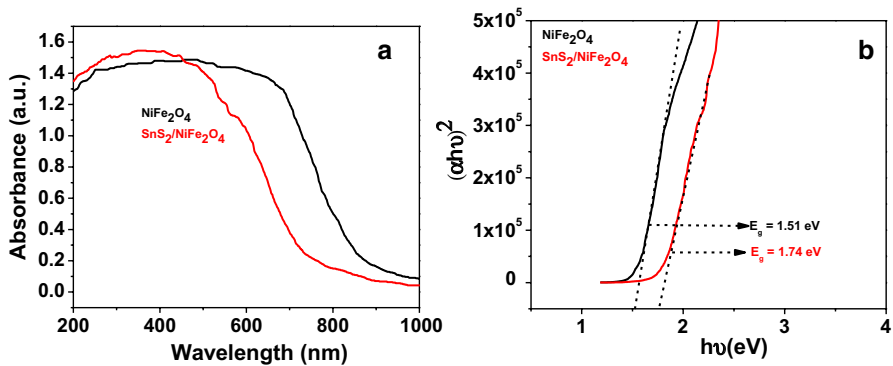**Fig. 3** **a** UV–Visible absorption spectrum of NiFe$_2$O$_4$ and SnS$_2$/NiFe$_2$O$_4$ NCs and **b** Optical band gab of NiFe$_2$O$_4$ and SnS$_2$/NiFe$_2$O$_4$ NCs

Photoluminescence (PL) studies

The PL spectrum of NiFe$_2$O$_4$ and SnS$_2$/NiFe$_2$O$_4$ NCs is shown in Fig. 4. From the PL spectra, blue emission band at 331 nm is ascribed due to near band emission which may occur by their excitonic transition between the surface metal–ligand lattices [27]. The violet emission band at 427 nm is attributed owing to their exchange of electrons from the shallow donor level to the valence band [25]. In addition, green emission band located at 573 nm, which is create by its structural deficiency like oxygen vacancies with other vacancy related defects are generates in NiFe$_2$O$_4$ lattice [25]. As well as, outcome of the optical studies was evidently
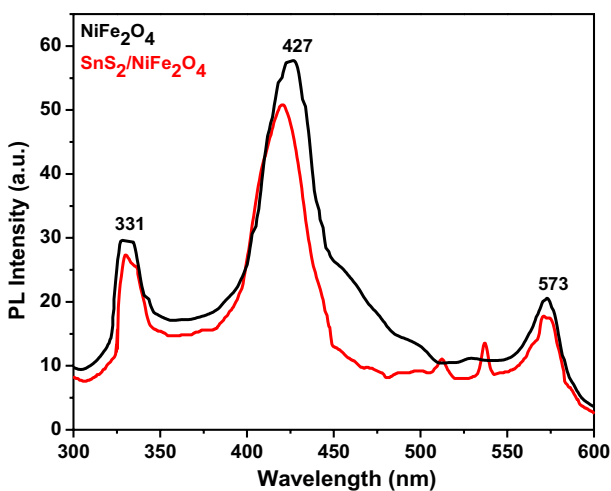

Fig. 4 PL spectrum of NiFe$_2$O$_4$ and SnS$_2$/NiFe$_2$O$_4$ NCs

demonstrated that the formation of heterojunction between the $NiFe_2O_4$ and SnS_2 nanoparticles greatly suppresses the photo excited electron–hole recombination.

Morphological analysis

The surface morphologies of $SnS_2/NiFe_2O_4$ NCs were examined through the FESEM analysis presented in Fig. 5a–d. The morphology of $SnS_2/NiFe_2O_4$ NCs

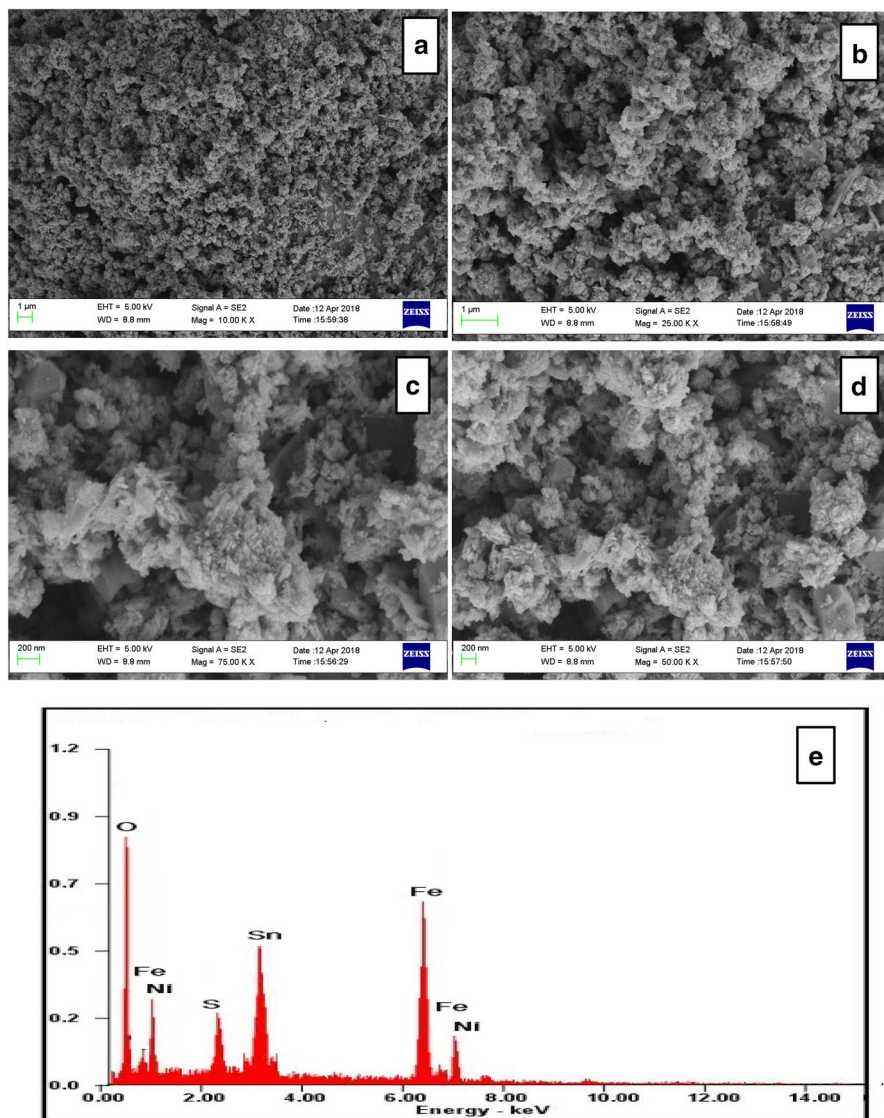Fig. 5 Different magnification FESEM images of (**a–d**) $SnS_2/NiFe_2O_4$ NCs and **e** EDAX spectrum of $SnS_2/NiFe_2O_4$ NCs

is seems to be sponge-like structure. From the images, sizes of the particles are obtained to be 50 to 100 nm. From the EDAX spectrum, elemental arrangements were investigated (Fig. 5d). The obtained result revealed the presence of Sn, Ni, Fe and O elements only, and no other elements were observed. This primarily confirms that the prepared material has high purity.

Photocatalytic behavior of as-prepared samples

A certain concentration of methylene blue (MB) and rhodamine B (RhB) as mentioned in "Experimental procedure for Photocatalytic test" section was taken separately and utilized as an organic pollutant. The beakers containing dye solution and photocatalyst were kept in dark for 60 min. under vigorous stirring to achieve adsorption/desorption equilibrium. After that, the beakers are exposed to sunlight by keeping it in an open terrace. For every 20 min, the aliquots of each dye solution were collected and subjected to UV spectroscopy to analyze the degradation mechanism. The photocatalytic activity is based on the principle that, a semiconductor material is irradiated with a light source, the electron in the valence band of that material will absorb the sufficient energy greater or equal to that of the band gap energy, shifts from the valence band to the conduction band and leaving the hole behind [23]. Normally the photocatalytic reduction of dye molecules will occur due to some main chemical reactions namely, the advanced oxidation process, that is, the emergence of hydroxyl radicals (˙OH) in a suit during the reaction process [25]. The (˙OH) radicals are one of the active species produced during the reaction between the holes behind in the semiconductor photocatalyst and the water molecules [25]. On the other side, the photo-exited electrons will react with the oxygen and to produce superoxide anions (O$_2^-$) which are also a key factor for the reduction of dye molecules [25]. In this case, because of the presence of ferrite molecule, there may be a chance of Fenton process has also occurred. Figure 6 shows the time-dependent UV-absorption curve for SnS$_2$/NiFe$_2$O$_4$ nanocomposite. From the figure, it is observed that the intensity of the peak associated with the dye solution is gradually decreases with the increase in irradiation time, this means that the dye
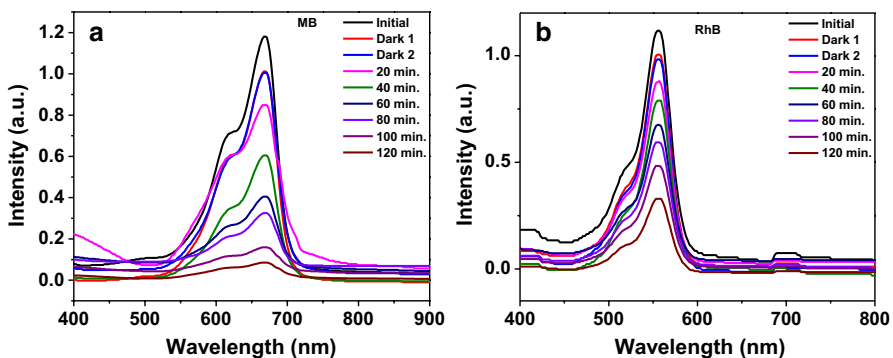

Fig. 6 Time-dependent UV–Vis absorption spectra for the reduction of (**a**) MB and **b** RhB with catalyst of SnS$_2$/NiFe$_2$O$_4$ NCs

molecules are mineralized due to the photocatalytic behavior of the synthesized material. Figure 7 shows the comparative difference in the concentration of the dye solution with respect to time for both $NiFe_2O_4$ and $SnS_2/NiFe_2O_4$ nanocomposite material, from that it is clear that the composite material shows better photocatalytic activity than that of the pure material, which is also clearly evident in the UV and PL studies. Because, composite material has slightly lower emission intensity as well as band gap energy was higher compared to pure one. This confirms the rate of electron–hole recombination is lowered, and thus it promotes the emergence of more hydroxyl radicals as well as superoxide anions which improves the photocatalytic activity [22]. The percentage of degradation for MB and RhB dye was determined to be 66% and 90% for $NiFe_2O_4$ and $SnS_2/NiFe_2O_4$, also 58% and 70% in the case of RhB dye within 120 min. On the basis of the above experimental results and discussion, a proposed mechanism for the enhanced photocatalytic activity over the present $SnS_2/NiFe_2O_4$ is shown schematically in Fig. 8. The possible photocatalytic reaction mechanism is shown in Fig. 8. From the observed Fig., photogenerated electrons in the CB of SnS_2 can transfer to the CB of $NiFe_2O_4$. Simultaneously, photogenerated holes in the VB of $NiFe_2O_4$ can be move around to the VB of SnS_2. Consequently, photogenerated electrons and holes move to different sides. This can boost up separation of electron–hole charge pairs and improves the photocatalytic activity. These are the reasons for the composite material showing good photocatalytic behavior than that of the pure material. The reaction kinetics of the as-prepared samples in the performance of degradation was quantitatively estimated from the Langmuir–Hinshelwood model which is obtained by plotting a graph between $\ln (C/C_0)$ and reaction time as represented in Fig. 9. This provides details about the average amount of dye molecules degrade per second.
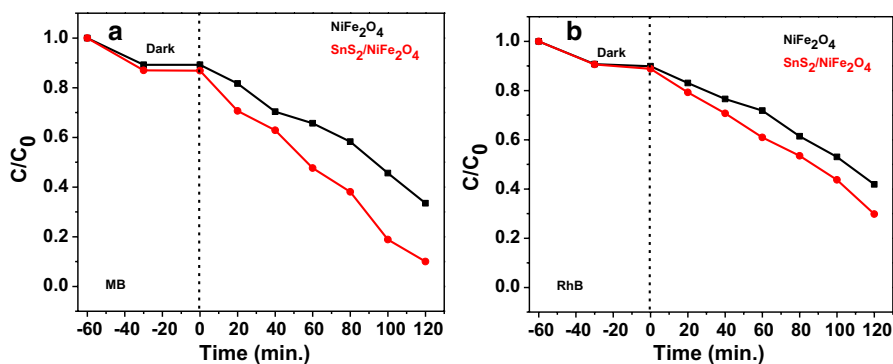
$$ln\left(\frac{c}{c_0}\right) = kt$$

Fig. 7 Time vs. concentration of (**a**) MB and **b** RhB with catalyst of $NiFe_2O_4$ and $SnS_2/NiFe_2O_4$ NCs

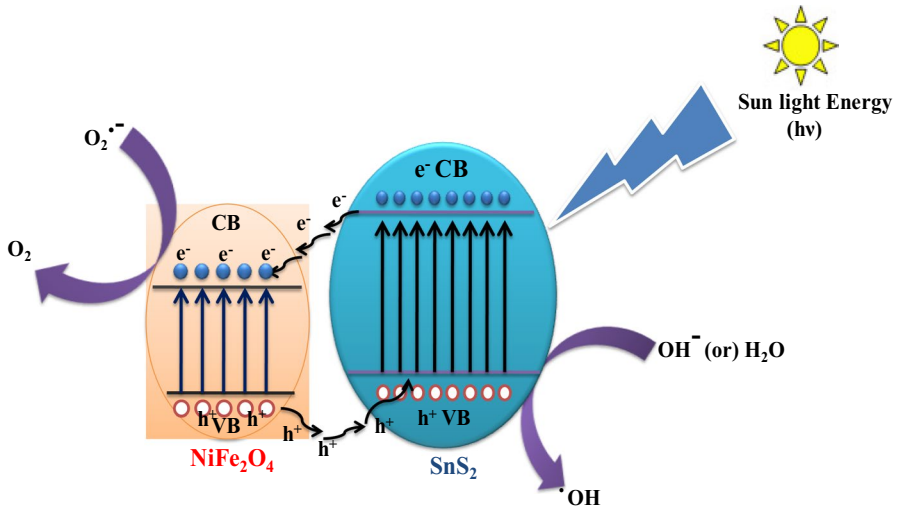**Fig. 8** Schematic illustration of the proposed reaction mechanism for the photocatalytic degradation of the MB and RhB dyes in the presence of SnS$_2$/NiFe$_2$O$_4$ NCs
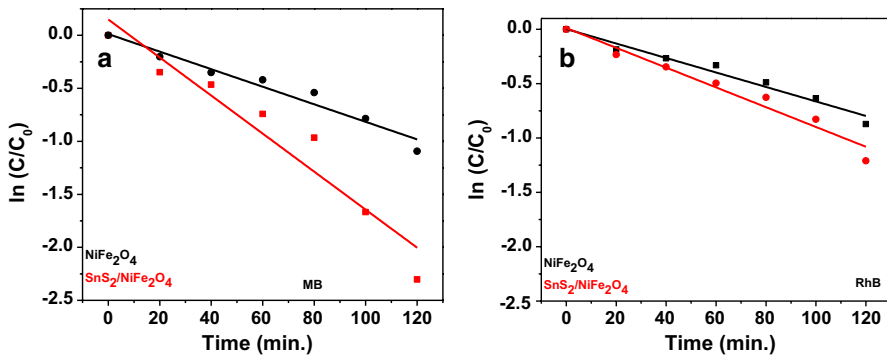

Fig. 9 Time vs. rate constant for (**a**) MB and **b** RhB with catalyst of NiFe$_2$O$_4$ and SnS$_2$/NiFe$_2$O$_4$ NCs

The rate constant, percentage of degradation, and the R^2 values of the prepared samples are narrated in Table 1.

Active species scavenger and reusable experiment

The active species are act as a crucial role in the dye degradation process. Hence, ·OH radical scavenger and O2$^-$ anion scavenger were studied by isopropyl alcohol (IPA) and para benzoquinone (PBQ). Figure 10 shows the variation of C/C$_0$ of MB and RhB as a function of irradiation time before and after scavengers were added into the photocatalytic system. In this experimental studies, 0.025 M of PBQ and 2 ml of IPA were mixed with the dye solution along with SnS$_2$/NiFe$_2$O$_4$ catalyst.

Table 1 Table of dye degradation efficiency, rate constant and R^2 values of $NiFe_2O_4$ and $SnS_2/NiFe_2O_4$ NCs

Dye	Samples	Rate constant (k) (s^{-1})	(R^2) value
Methylene blue	$NiFe_2O_4$	8.28×10^{-3}	0.94995 (66%)
	$NiFe_2O_4/SnS_2$	17.95×10^{-3}	0.91375 (90%)
Rhodamine B	$NiFe_2O_4$	6.67×10^{-3}	0.96339 (58%)
	$NiFe_2O_4/ SnS_2$	9.11×10^{-3}	0 .95595 (70%)
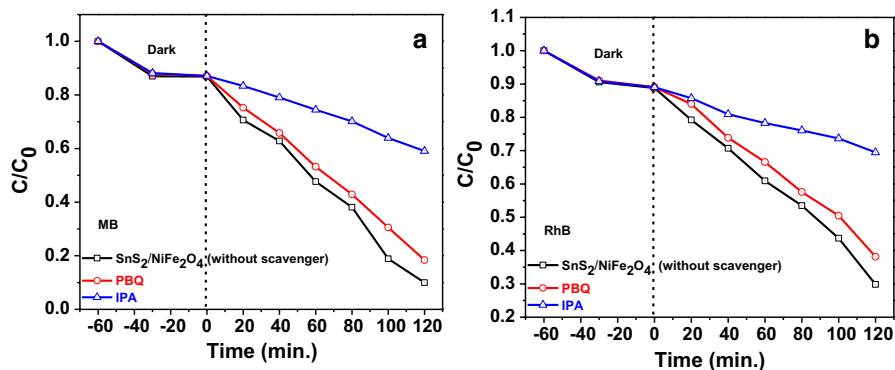
Fig. 10 a Scavenger experiment for 15 mg/l of MB dye. **b** Scavenger experiment for 10 mg/l of RhB dye

From the result, degradation percentage of dyes was radically reduced for IPA scavenger than that of PBQ. Therefore, it is concluded that the large number of ·OH radicals were generated when $SnS_2/NiFe_2O_4$ NCs was irradiated under sun light and played an important role in the degradation of the dye's active species. The degradation rates are 89.7%, 88.2%, 85.5%, 80.3%, 77.8% and 69.4%, 67.7%, 65.3%, 60.9%, 56.1%, respectively, for MB and RhB dyes. In reusability of $SnS_2/NiFe_2O_4$ NCs, degradation efficiency was slightly decreased in 4th and 5th consecutive rounds, respectively, for MB and RhB dyes which are shown in Fig. 11. From the observed result, it is noted that the $SnS_2/NiFe_2O_4$ NCs material demonstrates superior performance up to three cycles.

Conclusion

The as-prepared $SnS_2/NiFe_2O_4$ NCs were fabricated by two-step approach for photocatalytic activity. The sponge-like morphologies were attained from the developed composite materials and size was around to be 50–100 nm. In photocatalytic degradation studies, the degradation efficiency and rate constant of $SnS_2/NiFe_2O_4$ NCs are high at both the dyes due to creation of heterojunction between $NiFe_2O_4$ and SnS_2 assists to decrease the electron hole recombination capability as well as separation of charge carrier which enhance the sun light absorption of nanocomposite. Results
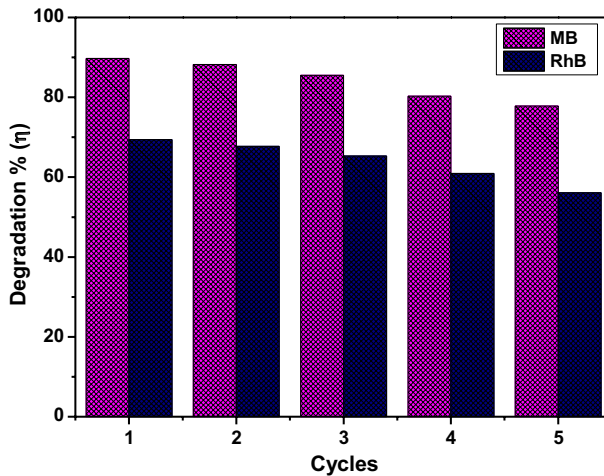
Fig. 11 Reusability chart of SnS$_2$/NiFe$_2$O$_4$ NCs

of the current study revealed the use of NCs in successful removal of organic pollutants from both domestic and industrially polluted water ecosystem.

References

1. P. Saharan, G.R. Chaudhary, S. Lata, S.K. Mehta, S. Mor, Ultrason. Sonochem. **22**, 317 (2015)
2. A. Fujishima, K. Honda, Nat. **238**, 37 (1972)
3. N. Nithya, G. Bhoopathi, G. Magesh, C.D.N. Kumar, Mater. Sci. Semicond. Process. **83**, 70 (2018)
4. M.W. Chang, C.C. Chung, J.M. Chern, T.S. Chen, Chem. Eng. Sci. **65**, 135 (2010)
5. S. Malato, P. Fernandez-Ibanez, M.I. Maldonado, J. Blanco, W. Gernjak, Catal. Today. **147**, 1 (2009)
6. S.F. Kang, C.H. Liao, S.T. Po, Chemosphere **41**, 1287 (2000)
7. J. Yu, X. Yu, Environ. Sci. Technol. **42**, 4902 (2008)
8. Y.Y. Yang, X.G. Zhang, C.G. Niu, H.P. Feng, P.Z. Qin, H. Guo, C. Liang, L. Zhang, H.Y. Liu, L. Li, Appl. Catalysis B Environ. **264**, 118465 (2020)
9. H. Guo, C.G. Niu, C.Y. Feng, C. Liang, L. Zhang, X.J. Wen, Y. Yang, H.Y. Liu, L. Li, L.S. Lin, Chem. Eng. J. **385**, 123919 (2020)
10. H. Guo, H.Y. Niu, C. Liang, C.G. Niu, Y. Liu, N. Tang, Y. Yang, H.Y. Liu, Y.Y. Yang, W.J. Wang, Chem. Eng. J. **401**, 126072 (2020)
11. J.T. Adeleke, T. Theivasanthi, M. Thiruppathi, M. Swaminathan, T. Akomolafe, A.B. Alabi, Appl. Surf. Sci. **455**, 195 (2018)
12. S.H. Chaki, M.P. Deshpande, D.P. Trivedi, J.P. Tailor, M.D. Chaudhary, K. Mahato, Appl. Nanosci. **3**, 189 (2013)
13. J. Srivind, V.S. Nagarethinam, M. Suganya, S. Balamurugan, K. Usharani, A.R. Balu, Vacuum **163**, 373 (2019)
14. Y.C. Zhang, Z.N. Du, S.Y. Li, M. Zhang, Appl. Catalysis B: Environ. **95**, 153 (2010)
15. A. Umar, M.S. Akhtar, G.N. Dar, M. Abaker, A.A. Hajry, S. Baskoutas, Talanta **114**, 183 (2013)
16. B. Palanivel, C. Ayappan, V. Jayaraman, S. Chidambaram, R. Maheswaran, A. Mani, Mater. Sci. Semicond. Process. **100**, 87 (2019)
17. F.A. Hezam, O. Nur, M.A. Mustafa, Colloids Surf. A **592**, 124586 (2020)
18. H. Guo, H.Y. Niu, C. Liang, C.G. Niu, D.W. Huang, L. Zhang, N. Tang, Y. Yang, C.Y. Feng, G.M. Zeng, J. Catalysis **370**, 289 (2019)

19. S. Annathurai, S. Chidambaram, B. Baskaran, G.P. Venkatesan, J. Inorg. Organomet. Polym. Mater. **29**, 535 (2019)
20. C. Vivek, B. Balraj, S. Thangavel, J. Mater. Sci.: Mater. Electron. **30**, 11220 (2019)
21. C. Vivek, B. Balraj, S. Thangavel, J. Electron. Mater. **49**, 1075 (2020)
22. M.J. Abel, A. Pramothkumar, N. Senthilkumar, K. Jothivenkatachalam, P.F.H. Inbaraj, J.J. Prince, Phys. B Condensed Matter. **572**, 117 (2019)
23. M.J. Abel, A. Pramothkumar, V. Archana, N. Senthilkumar, K. Jothivenkatachalam, J.J. Prince, Res. Chem. Intermed. **46**, 3509 (2020)
24. N. Senthilkumar, M. Ganapathy, A. Arulraj, M. Meena, M. Vimalan, I.V. Potheher, J. Alloys Comp. **750**, 171 (2018)
25. A. Lassoued, M.S. Lassoued, B. Dkhil, S. Ammar, A. Gadri, J. Mater. Sci. Mater. Electron. **29**, 7057 (2018)
26. K. Kombaiah, J.J. Vijaya, L.J. Kennedy, K. Kaviyarasu, Mater. Chem. Phys. **221**, 11 (2019)
27. B. Saravana Kumar, S. Muthu Lakshmi, G. Ravi, V. Ganesh, A. Sakunthala, R. Yuvakkumar, J. Alloys Comp. **723**, 115 (2017)

Publisher's Note Springer Nature remains neutral with regard to jurisdictional claims in published maps and institutional affiliations.